



# LUND UNIVERSITY

## Computation of radome reference cases using a rotationally symmetric full wave solver

Sjöberg, Daniel

2022

[Link to publication](#)

*Citation for published version (APA):*

Sjöberg, D. (2022). *Computation of radome reference cases using a rotationally symmetric full wave solver*. (Technical Report LUTEDX/(TEAT-7273)/1-23/(2022) ; Vol. TEAT-7273 ). Electromagnetic Theory Department of Electrical and Information Technology Lund University Sweden.

*Total number of authors:*

1

### General rights

Unless other specific re-use rights are stated the following general rights apply:

Copyright and moral rights for the publications made accessible in the public portal are retained by the authors and/or other copyright owners and it is a condition of accessing publications that users recognise and abide by the legal requirements associated with these rights.

- Users may download and print one copy of any publication from the public portal for the purpose of private study or research.
- You may not further distribute the material or use it for any profit-making activity or commercial gain
- You may freely distribute the URL identifying the publication in the public portal

Read more about Creative commons licenses: <https://creativecommons.org/licenses/>

### Take down policy

If you believe that this document breaches copyright please contact us providing details, and we will remove access to the work immediately and investigate your claim.

LUND UNIVERSITY

PO Box 117  
221 00 Lund  
+46 46-222 00 00

# Computation of radome reference cases using a rotationally symmetric full wave solver

Daniel Sjöberg

Electromagnetic Theory  
Department of Electrical and Information Technology  
Lund University  
Sweden



Daniel Sjöberg  
daniel.sjoberg@eit.lth.se

Department of Electrical and Information Technology  
Electromagnetic Theory  
Lund University  
P.O. Box 118  
SE-221 00 Lund  
Sweden

This is an author produced preprint version as part of a technical report series from the Electromagnetic Theory group at Lund University, Sweden. Homepage <http://www.eit.lth.se/teat>

Editor: Mats Gustafsson  
© Daniel Sjöberg, Lund, May 18, 2022

## Abstract

We demonstrate how to compute radome reference cases for benchmarking radome codes. Radomes are electrically large structures, and to facilitate the computations a rotationally symmetric structure is assumed. We show how to implement this in the commercial software Comsol Multiphysics, and how to extract the relevant data for comparison. Two example geometries are analyzed: a spherical shell radome, and an ogive shaped radome. In each case, the radome is in the order of ten wavelengths, but it is still possible to simulate on a regular laptop platform in about a minute. Using a platform with more memory and spending more time to simulate more modes and synthesize the results, reference cases for even larger radomes with realistic feeds can be simulated, which is suggested as a topic for future studies. Results for an ogive shaped radome with a diameter of 30 and 50 wavelengths using a highly symmetrical antenna are provided.

## 1 Introduction

The word “radome” is constructed from “radar dome”, and denotes a structure covering an antenna in order to protect it from the surrounding environment, where for instance wind and rain may be detrimental factors. It is usually constructed as a relatively thin shell, either as a single solid material or as a composite structure entailing several layers. A particular challenge for the radome is to enable the antenna to transmit efficiently in its band of operation. The simplest design is to make the thickness of the radome to correspond to half a wavelength (scaled to the material) [4]. However, this may lead to excessively heavy structures, promoting composite structures, where for instance a thick but light-weight core material is sandwiched between two thin but hard shells [4]. To enable further control of the electromagnetic properties, metallic patterns may be used to achieve stronger frequency selectivity [7].

Radomes are electrically large, typically many tens of wavelengths. This makes their design computationally challenging, and a lot of effort has been put on developing simulation tools to evaluate their performance. In many cases, the radome geometry is rotationally symmetric, which simplifies the problem significantly if also the antenna can be assumed highly symmetric. In this report, we demonstrate how a commercial code like Comsol Multiphysics may be used to simulate rotationally symmetric structures in order to provide reference data for in-house developed radome simulation codes. For structures with spherical symmetry, an additional reference code based on spherical vector waves has been developed [5, 6]. The results have been compared with results from this report and the SmartRAT code developed by Saab Dynamics in [2].

This report is structured as follows. In Section 2, we present the specific form of Maxwell’s equations in cylindrical coordinates, and the expansion of the fields in azimuthal modes. We also exemplify how a linearly polarized field can be represented by a single azimuthal mode under certain conditions, providing a practical reference case with a relatively small numerical cost. In Section 3, we give expressions for how

to compute the farfield amplitude for arbitrary azimuthal modes, as well as some special cases. Detailed derivations are given in Appendix A. In Section 4, we discuss the implementation in Comsol Multiphysics, and in Sections 5 and 6 we provide examples of the computations for a spherical radome, as well as a more realistically shaped ogive radome in various sizes. Finally, conclusions are provided in Section 7.

## 2 Rotational symmetry

In order to conserve the computational size of the problem to be simulated, we may consider a rotationally symmetric structure, which in principle converts the problem from 3D to 2D. This is a huge saving in computational complexity, but since an arbitrary excitation involves all azimuthal modes, we typically need to solve for very many modes and synthesize the resulting solution as a superposition of the modes, which renders the name “2.5D” for the resulting dimensional complexity of the problem. In order to reduce the number of modes solved for, we can also require symmetry from the excitation. Typically, we restrict the antenna to radiate along the axis of rotational symmetry ( $z$ -axis) with linear or circular polarization, requiring only one azimuthal mode.

### 2.1 Representation in cylindrical coordinates

For a rotationally symmetric structure, it is beneficial to express the fields in cylindrical coordinates  $(\rho, \varphi, z)$  as

$$\mathbf{E}(\mathbf{r}) = \sum_{m=-\infty}^{\infty} [E_{\rho}^{(m)}(\rho, z)\hat{\boldsymbol{\rho}} + E_{\varphi}^{(m)}(\rho, z)\hat{\boldsymbol{\varphi}} + E_z^{(m)}(\rho, z)\hat{\mathbf{z}}] e^{-jm\varphi} \quad (2.1)$$

$$\mathbf{H}(\mathbf{r}) = \sum_{m=-\infty}^{\infty} [H_{\rho}^{(m)}(\rho, z)\hat{\boldsymbol{\rho}} + H_{\varphi}^{(m)}(\rho, z)\hat{\boldsymbol{\varphi}} + H_z^{(m)}(\rho, z)\hat{\mathbf{z}}] e^{-jm\varphi} \quad (2.2)$$

This representation is valid for any structure, but for a rotationally symmetric structure there is no coupling between the azimuthal modes and we may consider each mode index  $m$  separately in Maxwell’s equations. The curl operation can be written in cylindrical coordinates as

$$\nabla \times \mathbf{E} = \hat{\boldsymbol{\rho}} \left( \frac{1}{\rho} \frac{\partial E_z}{\partial \varphi} - \frac{\partial E_{\varphi}}{\partial z} \right) + \hat{\boldsymbol{\varphi}} \left( \frac{\partial E_{\rho}}{\partial z} - \frac{\partial E_z}{\partial \rho} \right) + \hat{\mathbf{z}} \left( \frac{1}{\rho} \frac{\partial}{\partial \rho} (\rho E_{\varphi}) - \frac{1}{\rho} \frac{\partial E_{\rho}}{\partial \varphi} \right) \quad (2.3)$$

Maxwell’s equations in isotropic space,  $\nabla \times \mathbf{E} = -j\omega\mu\mathbf{H}$  and  $\nabla \times \mathbf{H} = j\omega\epsilon\mathbf{E}$ , can then be written

$$-\frac{jm}{\rho} E_z^{(m)} - \frac{\partial E_{\varphi}^{(m)}}{\partial z} = -j\omega\mu H_{\rho}^{(m)} \quad -\frac{jm}{\rho} H_z^{(m)} - \frac{\partial H_{\varphi}^{(m)}}{\partial z} = j\omega\epsilon E_{\rho}^{(m)} \quad (2.4)$$

$$\frac{\partial E_{\rho}^{(m)}}{\partial z} - \frac{\partial E_z^{(m)}}{\partial \rho} = -j\omega\mu H_{\varphi}^{(m)} \quad \frac{\partial H_{\rho}^{(m)}}{\partial z} - \frac{\partial H_z^{(m)}}{\partial \rho} = j\omega\epsilon E_{\varphi}^{(m)} \quad (2.5)$$

$$\frac{1}{\rho} \frac{\partial}{\partial \rho} (\rho E_{\varphi}^{(m)}) + \frac{jm}{\rho} E_{\rho}^{(m)} = -j\omega\mu H_z^{(m)} \quad \frac{1}{\rho} \frac{\partial}{\partial \rho} (\rho H_{\varphi}^{(m)}) + \frac{jm}{\rho} H_{\rho}^{(m)} = j\omega\epsilon E_z^{(m)} \quad (2.6)$$

It is seen that only for  $m = 0$  do these equations split into an in-plane electric field mode  $(E_\rho^{(0)}, E_z^{(0)}, H_\varphi^{(0)})$ , and an out-of-plane electric field mode  $(E_\varphi^{(0)}, H_\rho^{(0)}, H_z^{(0)})$ . For  $m \neq 0$ , we need to solve for all field components.

## 2.2 Synthesizing linear polarization

We are primarily interested in linearly polarized antennas, which can be studied as a superposition of  $m = +1$  and  $m = -1$ . When the excitations of the positive and negative azimuthal modes are given symmetrically in  $\rho$  and  $z$  and anti-symmetrically in  $\varphi$ ,

$$\mathbf{E}_0^{(\pm m)}(\rho, z) = [E_{0\rho}^{(+m)}(\rho, z)\hat{\boldsymbol{\rho}} \pm E_{0\varphi}^{(+m)}(\rho, z)\hat{\boldsymbol{\varphi}} + E_{0z}^{(+m)}(\rho, z)\hat{\boldsymbol{z}}]e^{\mp jm\varphi} \quad (2.7)$$

where  $[E_{0\rho}^{(+m)}(\rho, z), E_{0\varphi}^{(+m)}(\rho, z), E_{0z}^{(+m)}(\rho, z)]$  represent the spatial distribution of the excitation, we find the parity rules

$$(E_\rho^{(+m)}, E_z^{(+m)}, H_\varphi^{(+m)}) = (E_\rho^{(-m)}, E_z^{(-m)}, H_\varphi^{(-m)}) \quad (2.8)$$

$$(E_\varphi^{(+m)}, H_\rho^{(+m)}, H_z^{(+m)}) = -(E_\varphi^{(-m)}, H_\rho^{(-m)}, H_z^{(-m)}) \quad (2.9)$$

Hence, an excitation that is a superposition of  $\mathbf{E}_0^{(\pm m)}$ , that is, symmetric in  $\rho$  and  $z$  and antisymmetric in  $\varphi$ ,

$$\mathbf{E}_0 = \sum_{m=1}^{\infty} \alpha_m \mathbf{E}_0^{(+m)} + \beta_m \mathbf{E}_0^{(-m)} \quad (2.10)$$

can be computed from the results of a positive azimuthal mode  $+m$  only, as

$$\mathbf{E}(\mathbf{r}) = \sum_{m=-\infty}^{\infty} [E_\rho^{(m)}(\rho, z)\hat{\boldsymbol{\rho}} + E_\varphi^{(m)}(\rho, z)\hat{\boldsymbol{\varphi}} + E_z^{(m)}(\rho, z)\hat{\boldsymbol{z}}] e^{-jm\varphi} \quad (2.11)$$

$$= \sum_{m=1}^{\infty} \left\{ E_\rho^{(+m)}(\rho, z)[\alpha_m e^{-jm\varphi} + \beta_m e^{+jm\varphi}]\hat{\boldsymbol{\rho}} \right. \quad (2.12)$$

$$+ E_\varphi^{(+m)}(\rho, z)[\alpha_m e^{-jm\varphi} - \beta_m e^{+jm\varphi}]\hat{\boldsymbol{\varphi}} \quad (2.13)$$

$$\left. + E_z^{(+m)}(\rho, z)[\alpha_m e^{-jm\varphi} + \beta_m e^{+jm\varphi}]\hat{\boldsymbol{z}} \right\} \quad (2.14)$$

$$\mathbf{H}(\mathbf{r}) = \sum_{m=-\infty}^{\infty} [H_\rho^{(m)}(\rho, z)\hat{\boldsymbol{\rho}} + H_\varphi^{(m)}(\rho, z)\hat{\boldsymbol{\varphi}} + H_z^{(m)}(\rho, z)\hat{\boldsymbol{z}}] e^{-jm\varphi} \quad (2.15)$$

$$= \sum_{m=1}^{\infty} \left\{ H_\rho^{(+m)}(\rho, z)[\alpha_m e^{-jm\varphi} - \beta_m e^{+jm\varphi}]\hat{\boldsymbol{\rho}} \right. \quad (2.16)$$

$$+ H_\varphi^{(+m)}(\rho, z)[\alpha_m e^{-jm\varphi} + \beta_m e^{+jm\varphi}]\hat{\boldsymbol{\varphi}} \quad (2.17)$$

$$\left. + H_z^{(+m)}(\rho, z)[\alpha_m e^{-jm\varphi} - \beta_m e^{+jm\varphi}]\hat{\boldsymbol{z}} \right\} \quad (2.18)$$

In particular, for  $m = 1$  and circular polarization propagating along the  $z$ -axis, that is,  $E_{0\rho}^{(+)}(\rho, z) = E_0(\rho, z)$ ,  $E_{0\varphi}^{(+)}(\rho, z) = -jE_0(\rho, z)$ ,  $E_{0z}^{(+)} = 0$ , and  $\alpha_1 = \beta_1 = 1/2$ , the total excitation is linearly polarized,

$$\begin{aligned} \mathbf{E}_0 &= E_0(\rho, z) \frac{1}{2} [(e^{-j\varphi} + e^{j\varphi})\hat{\boldsymbol{\rho}} - j(e^{-j\varphi} - e^{j\varphi})\hat{\boldsymbol{\varphi}}] = E_0(\rho, z) [\cos(\varphi)\hat{\boldsymbol{\rho}} - \sin(\varphi)\hat{\boldsymbol{\varphi}}] \\ &= E_0(\rho, z)\hat{\boldsymbol{x}} \end{aligned} \quad (2.19)$$

and the total field can be computed from the positive azimuthal mode only:

$$\mathbf{E}(\mathbf{r}) = E_\rho^{(+)}(\rho, z) \cos(\varphi)\hat{\boldsymbol{\rho}} - jE_\varphi^{(+)}(\rho, z) \sin(\varphi)\hat{\boldsymbol{\varphi}} + E_z^{(+)}(\rho, z) \cos(\varphi)\hat{\boldsymbol{z}} \quad (2.20)$$

$$\mathbf{H}(\mathbf{r}) = -jH_\rho^{(+)}(\rho, z) \sin(\varphi)\hat{\boldsymbol{\rho}} + H_\varphi^{(+)}(\rho, z) \cos(\varphi)\hat{\boldsymbol{\varphi}} - jH_z^{(+)}(\rho, z) \sin(\varphi)\hat{\boldsymbol{z}} \quad (2.21)$$

Hence, we need only solve for the  $m = 1$  mode when computing results for linearly polarized fields propagating along the  $z$ -axis.

### 3 Farfield computations

The far field amplitude from tangential electric and magnetic fields on a general surface  $S$  with outward normal  $\hat{\boldsymbol{n}}$  is

$$\mathbf{F}(\hat{\boldsymbol{k}}) = \frac{jk}{4\pi} \hat{\boldsymbol{k}} \times \int_S [\mathbf{E}(\mathbf{r}) \times \hat{\boldsymbol{n}} + \eta_0 \hat{\boldsymbol{k}} \times (\hat{\boldsymbol{n}} \times \mathbf{H}(\mathbf{r}))] e^{jk\hat{\boldsymbol{k}} \cdot \mathbf{r}} dS \quad (3.1)$$

where  $k = \omega/c_0 = 2\pi/\lambda$  is the free space wavenumber (here,  $\omega = 2\pi f$  is the angular frequency at ordinary frequency  $f$ ,  $\lambda$  is the vacuum wavelength, and  $c_0$  the speed of light in vacuum, respectively), and  $\hat{\boldsymbol{k}}$  is the observation direction. In the specific case of a rotationally symmetric structure, the surface  $S$  is described by a curve  $\gamma$  in the  $\rho - z$  plane:

$$\begin{aligned} \mathbf{F}^{(m)}(\hat{\boldsymbol{k}}) &= \frac{jk}{4\pi} \hat{\boldsymbol{k}} \times \int_{\rho \in \gamma} \int_{\varphi=0}^{2\pi} [\mathbf{E}^{(m)}(\rho, z) \times \hat{\boldsymbol{n}} + \eta_0 \hat{\boldsymbol{k}} \times (\hat{\boldsymbol{n}} \times \mathbf{H}^{(m)}(\rho, z))] \\ &\quad e^{j(k\hat{\boldsymbol{k}} \cdot \mathbf{r} - m\varphi)} \rho d\varphi dl \end{aligned} \quad (3.2)$$

The integral in the  $\varphi$ -direction can be explicitly computed. We summarize below the results for arbitrary  $m$ ,  $m = 0$ , and synthesizing a linear polarization using  $m = \pm 1$ . Detailed derivations are given in Appendix A. The formulas have been compared with similar formulas in the literature, as in [3].

### 3.1 Arbitrary $m$

We start with the result for arbitrary  $m$  as derived in Appendix A.1. For any direction  $(\theta, \phi)$ , we have

$$\begin{aligned}
\mathbf{F}^{(m)}(\theta, \phi) = & \hat{\boldsymbol{\theta}} \frac{j^k}{2} j^m e^{-jm\phi} \int_{\rho \in \gamma} \left\{ - [C_m n_z E_\varphi^{(m)} - S_m (n_\rho E_z^{(m)} - n_z E_\rho^{(m)})] \sin \phi \right. \\
& + [S_m n_z E_\varphi^{(m)} + C_m (n_\rho E_z^{(m)} - n_z E_\rho^{(m)})] \cos \phi \\
& - \eta_0 [C_m n_z H_\varphi^{(m)} - S_m (n_\rho H_z^{(m)} - n_z H_\rho^{(m)})] \cos \theta \cos \phi \\
& - \eta_0 [S_m n_z H_\varphi^{(m)} + C_m (n_\rho H_z^{(m)} - n_z H_\rho^{(m)})] \cos \theta \sin \phi \\
& \left. + \eta_0 A_m n_\rho H_\varphi^{(m)} \sin \theta \right\} e^{jkz \cos \theta} \rho \, d\ell \\
& + \hat{\boldsymbol{\phi}} \frac{j^k}{2} j^m e^{-jm\phi} \int_{\rho \in \gamma} \left\{ - [C_m n_z E_\varphi^{(m)} - S_m (n_\rho E_z^{(m)} - n_z E_\rho^{(m)})] \cos \theta \cos \phi \right. \\
& - [S_m n_z E_\varphi^{(m)} + C_m (n_\rho E_z^{(m)} - n_z E_\rho^{(m)})] \cos \theta \sin \phi \\
& \quad + A_m n_\rho E_\varphi^{(m)} \sin \theta \\
& + \eta_0 [C_m n_z H_\varphi^{(m)} - S_m (n_\rho H_z^{(m)} - n_z H_\rho^{(m)})] \sin \phi \\
& \left. - \eta_0 [S_m n_z H_\varphi^{(m)} + C_m (n_\rho H_z^{(m)} - n_z H_\rho^{(m)})] \cos \phi \right\} e^{jkz \cos \theta} \rho \, d\ell \quad (3.3)
\end{aligned}$$

In Appendix A.2, the above expression is computed for the planes  $\phi = 0$  and  $\phi = \pi/2$ . In the plane  $\phi = 0$ ,  $0 < \theta < \pi$ , the far field amplitude is (this result has been verified against the expressions in [3])

$$\begin{aligned}
\mathbf{F}^{(m)}(\theta, \phi = 0) & = \hat{\boldsymbol{\theta}} \frac{j^k}{2} j^m \int_{\rho \in \gamma} \left\{ \left[ \frac{m J_m(k\rho \sin \theta)}{k\rho \sin \theta} n_z E_\varphi^{(m)} + j J'_m(k\rho \sin \theta) (n_\rho E_z^{(m)} - n_z E_\rho^{(m)}) \right] \right. \\
& - \eta_0 \left[ j J'_m(k\rho \sin \theta) n_z H_\varphi^{(m)} - \frac{m J_m(k\rho \sin \theta)}{k\rho \sin \theta} (n_\rho H_z^{(m)} - n_z H_\rho^{(m)}) \right] \cos \theta \\
& \left. + \eta_0 J_m(k\rho \sin \theta) n_\rho H_\varphi^{(m)} \sin \theta \right\} e^{jkz \cos \theta} \rho \, d\ell \\
& + \hat{\boldsymbol{\phi}} \frac{j^k}{2} j^m \int_{\rho \in \gamma} \left\{ \left[ -j J'_m(k\rho \sin \theta) n_z E_\varphi^{(m)} + \frac{m J_m(k\rho \sin \theta)}{k\rho \sin \theta} (n_\rho E_z^{(m)} - n_z E_\rho^{(m)}) \right] \cos \theta \right. \\
& \quad + J_m(k\rho \sin \theta) n_\rho E_\varphi^{(m)} \sin \theta \\
& \left. - \eta_0 \left[ \frac{m J_m(k\rho \sin \theta)}{k\rho \sin \theta} n_z H_\varphi^{(m)} + j J'_m(k\rho \sin \theta) (n_\rho H_z^{(m)} - n_z H_\rho^{(m)}) \right] \right\} e^{jkz \cos \theta} \rho \, d\ell \quad (3.4)
\end{aligned}$$



In the plane  $\phi = \pi/2$ ,  $0 < \theta < \pi$ , we have

$$\begin{aligned}
& \mathbf{F}^{(m)}(\theta, \phi = \pi/2) \\
&= \hat{\boldsymbol{\theta}} \frac{jk}{2} \int_{\rho \in \gamma} \left\{ \left[ \frac{m J_m(k\rho \sin \theta)}{k\rho \sin \theta} n_z E_\varphi^{(m)} + j J'_m(k\rho \sin \theta) (n_\rho E_z^{(m)} - n_z E_\rho^{(m)}) \right] \right. \\
&\quad - \eta_0 \left[ j J'_m(k\rho \sin \theta) n_z H_\varphi^{(m)} - \frac{m J_m(k\rho \sin \theta)}{k\rho \sin \theta} (n_\rho H_z^{(m)} - n_z H_\rho^{(m)}) \right] \cos \theta \\
&\quad \left. + \eta_0 J_m(k\rho \sin \theta) n_\rho H_\varphi^{(m)} \sin \theta \right\} e^{jkz \cos \theta} \rho d\ell \\
&+ \hat{\boldsymbol{\phi}} \frac{jk}{2} \int_{\rho \in \gamma} \left\{ - \left[ j J'_m(k\rho \sin \theta) n_z E_\varphi^{(m)} - \frac{m J_m(k\rho \sin \theta)}{k\rho \sin \theta} (n_\rho E_z^{(m)} - n_z E_\rho^{(m)}) \right] \cos \theta \right. \\
&\quad \left. + J_m(k\rho \sin \theta) n_\rho E_\varphi^{(m)} \sin \theta \right. \\
&\quad \left. + \eta_0 \left[ - \frac{m J_m(k\rho \sin \theta)}{k\rho \sin \theta} n_z H_\varphi^{(m)} - j J'_m(k\rho \sin \theta) (n_\rho H_z^{(m)} - n_z H_\rho^{(m)}) \right] \right\} e^{jkz \cos \theta} \rho d\ell
\end{aligned} \tag{3.5}$$

These expressions apply to any mode  $m$ .

### 3.2 Axial excitation, $m = 0$

In Appendix A.3, the following formula for the far field amplitude in a plane with arbitrary  $\phi$  and  $0 < \theta < \pi$  is derived:

$$\begin{aligned}
\mathbf{F}^{(0)}(\theta, \phi) &= \hat{\boldsymbol{\theta}} \frac{jk}{2} \int_{\rho \in \gamma} \left\{ -j(n_\rho E_z^{(0)} - n_z E_\rho^{(0)}) J_1(k\rho \sin \theta) + j\eta_0 n_z H_\varphi^{(0)} J_1(k\rho \sin \theta) \cos \theta \right. \\
&\quad \left. + \eta_0 J_0(k\rho \sin \theta) n_\rho H_\varphi^{(0)} \sin \theta \right\} e^{jkz \cos \theta} \rho d\ell \\
&+ \hat{\boldsymbol{\phi}} \frac{jk}{2} \int_{\rho \in \gamma} \left\{ jn_z E_\varphi^{(0)} J_1(k\rho \sin \theta) \cos \theta + J_0(k\rho \sin \theta) n_\rho E_\varphi^{(0)} \sin \theta \right. \\
&\quad \left. + j\eta_0 (n_\rho H_z^{(0)} - n_z H_\rho^{(0)}) J_1(k\rho \sin \theta) \right\} e^{jkz \cos \theta} \rho d\ell \tag{3.6}
\end{aligned}$$

It is seen that the field is independent of  $\phi$  except for the direction of the unit vector  $\hat{\boldsymbol{\phi}}$ , that is, it is rotationally symmetric as expected.

### 3.3 Synthesized linear excitation, $m = 1$

Finally, in Appendix A.4, the far field formulas in the E-plane and the H-plane are derived for linearly polarized excitation. For the E-plane ( $\phi = 0$ ,  $0 < \theta < \pi$ ), the

result is

$$\begin{aligned} \mathbf{F}_E(\theta) = \hat{\boldsymbol{\theta}} \frac{jk}{2} \int_{\rho \in \gamma} \left\{ \left[ \frac{J_1(k\rho \sin \theta)}{k\rho \sin \theta} n_z E_\varphi^{(1)} + j J_1'(k\rho \sin \theta) (n_\rho E_z^{(1)} - n_z E_\rho^{(1)}) \right] \right. \\ \left. - \eta_0 \left[ j J_1'(k\rho \sin \theta) n_z H_\varphi^{(1)} - \frac{J_1(k\rho \sin \theta)}{k\rho \sin \theta} (n_\rho H_z^{(1)} - n_z H_\rho^{(1)}) \right] \cos \theta \right. \\ \left. + \eta_0 J_1(k\rho \sin \theta) n_\rho H_\varphi^{(1)} \sin \theta \right\} e^{jkz \cos \theta} \rho \, d\ell \quad (3.7) \end{aligned}$$

In the H-plane ( $\phi = \pi/2$ ,  $0 < \theta < \pi$ ), we have

$$\begin{aligned} \mathbf{F}_H(\theta) = \hat{\boldsymbol{\phi}} \frac{jk}{2} \int_{\rho \in \gamma} \left\{ - \left[ j J_1'(k\rho \sin \theta) n_z E_\varphi^{(1)} - \frac{J_1(k\rho \sin \theta)}{k\rho \sin \theta} (n_\rho E_z^{(1)} - n_z E_\rho^{(1)}) \right] \cos \theta \right. \\ \left. + J_1(k\rho \sin \theta) n_\rho E_\varphi^{(1)} \sin \theta \right. \\ \left. + \eta_0 \left[ - \frac{J_1(k\rho \sin \theta)}{k\rho \sin \theta} n_z H_\varphi^{(1)} - j J_1'(k\rho \sin \theta) (n_\rho H_z^{(1)} - n_z H_\rho^{(1)}) \right] \right\} e^{jkz \cos \theta} \rho \, d\ell \quad (3.8) \end{aligned}$$

It is seen that in the E-plane the field is purely in the  $\hat{\boldsymbol{\theta}}$ -direction, and in the H-plane it is purely in the  $\hat{\boldsymbol{\phi}}$ -direction. This is due to the linearly polarized excitation and the rotational symmetry of the structure.

## 4 Implementation in Comsol Multiphysics

Solving Maxwell's equations in a rotational symmetric setting is straightforward in a commercial program like Comsol Multiphysics. All that has to be done is to choose the azimuthal index  $m$  and define the geometry, material parameters, and the port settings, in a 2D geometry, see Figure 1. However, the infrastructure for setting up a multimodal excitation and summing the results for different modes is at present not straightforward, and we have resolved to using a very small number of azimuthal modes in order to generate reference data. However, these sets of data should still be quite valuable to benchmark the codes from Saab Dynamics.

In the top part of Figure 1, we see how to set the azimuthal mode number  $m$  in the physics module *Electromagnetic Waves, Frequency Domain*. The region with green color is a Perfectly Matched Layer (PML), which is a numerical implementation of an absorbing boundary condition allowing propagating waves to escape the computational domain without being reflected.

In the lower part of Figure 1, we see that the exciting antenna is defined as a PEC-backed port, with an electric mode field given as (in Comsol the cylindrical radius  $\rho$  is named 'r')

$$\mathbf{E}_{\text{port}} = \cos(\pi\rho/w)(\hat{\boldsymbol{\rho}} - j\hat{\boldsymbol{\phi}}) \quad (4.1)$$

where  $w$  is the diameter of the antenna. This corresponds to a linearly polarized circular antenna with a cosine-tapering in the radial direction. The amplitude tapering

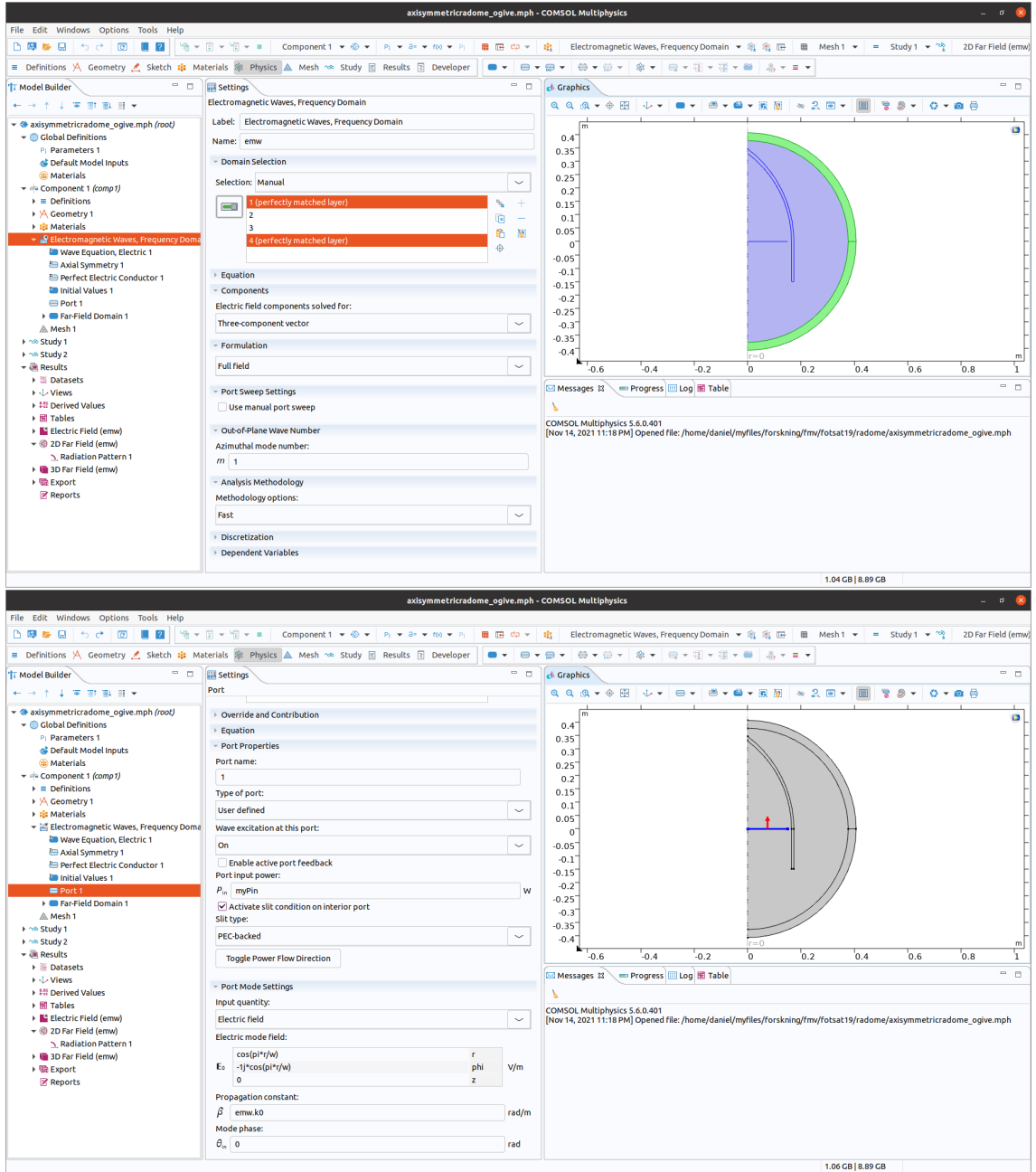


Figure 1: Some settings in Comsol Multiphysics, including azimuthal mode index  $m = 1$ , PML region, and port settings.

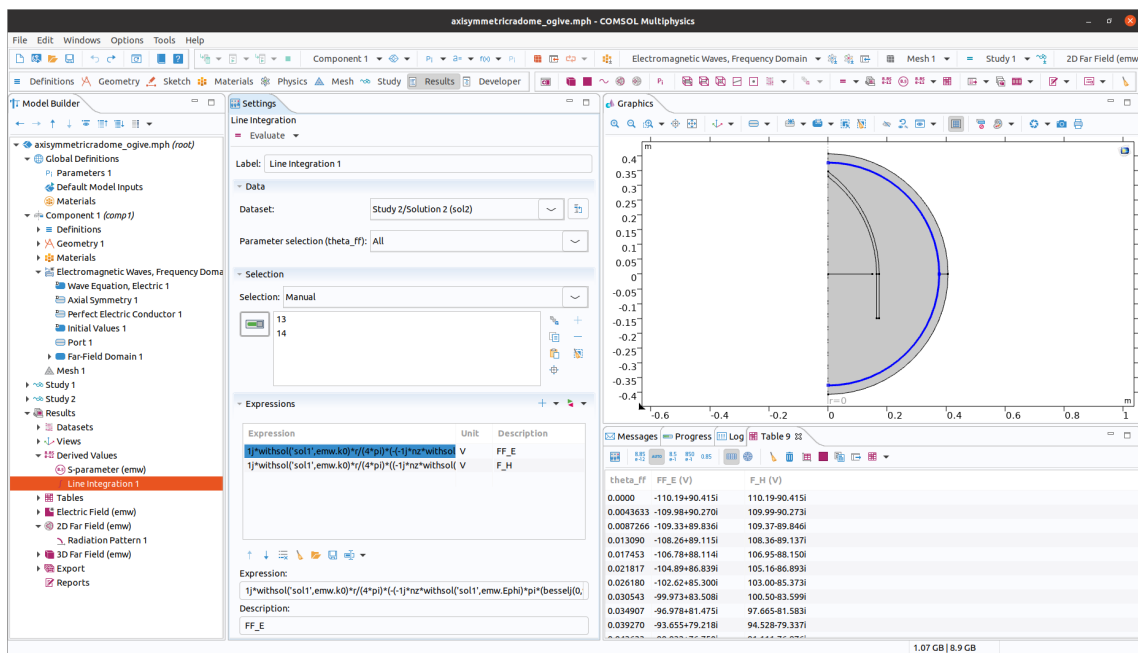


Figure 2: Computational settings for farfield in Comsol Multiphysics.

helps in reducing the sidelobes of the antenna. When shrinking the width  $w$  of the antenna to a very small number compared to wavelength  $\lambda$ , a dipole excitation is achieved regardless of the tapering.

Further, the far field integration needs to be implemented. This can be done in postprocessing by using the possibility to set up a line integration as shown in Figure 2. Formulas like (3.7) and (3.8) can be explicitly provided in the Graphical User Interface (GUI). One thing to watch out for is that if there are parameter sweeps or multiple studies activated, there are several solutions stored in Comsol. One way of choosing which solution to use in the integrals, is to use the command 'withsol()'. A particular circumstance is that the formulas are quite long, and the final expression to integrate may be in the order of tens of lines of code. In order to handle the input, we have typed the expressions in a separate text editor where more advanced 'search and replace' operations are available, and then copy-pasted the final expression into the Comsol GUI.

When the far field results have been computed into a table as seen in the lower right part of the screen shot in Figure 2, they can be exported in text format to a file which can be exchanged between organizations to facilitate comparisons between different computational methods.

In the following, we give examples of radome geometries analyzed with Comsol as described above.

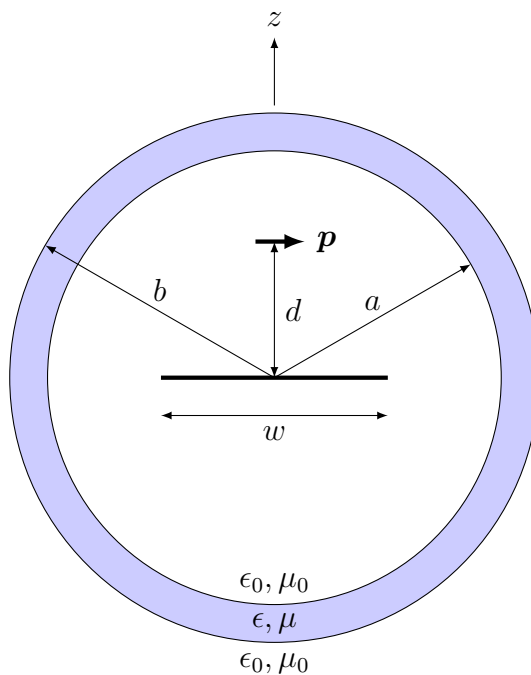


Figure 3: Geometry parameters of the spherical radome. The antenna consists of a small horizontally polarized electric dipole  $\mathbf{p}$  on the  $z$ -axis at distance  $d$  from a reflector of width  $w$  at the origin. The radome thickness is  $t = b - a$ .

## 5 Example: spherical radome

The simplest geometry is a spherical radome. This has been analyzed using expansions in spherical vector waves in [6], and using SmartRAT in [2]. The geometry parameters are defined in Figure 3. Several comparisons between the methods for many different geometries are given in [2]. In this document, we provide only a representative example of a relatively large radome.

The parameters of the problem are (not to scale of Figure 3)

- $f_0 = 10$  GHz (frequency)
- $\lambda_0 = c_0/f_0$  (wavelength)
- $a = 10\lambda_0$  (inner radius of radome)
- $t = \lambda_0/4$  (thickness of radome)
- $b = a + t$  (outer radius of radome)
- $w = 3\lambda_0$  (diameter of PEC disk)
- $d = 1.8\lambda_0$  (distance from origin to dipole)
- $\epsilon_r = \epsilon/\epsilon_0 = 3(1 - 0.01j)$ ,  $\mu_r = \mu/\mu_0 = 1$  (relative permittivity and permeability of radome)

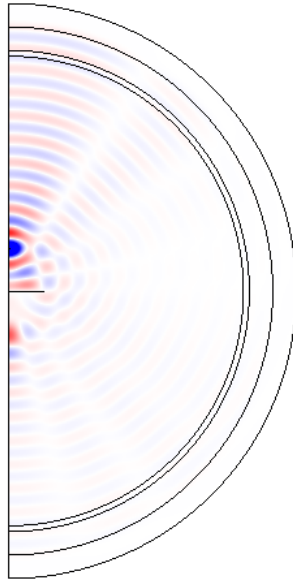


Figure 4: Fields of a reflector-backed dipole antenna inside a spherical radome.

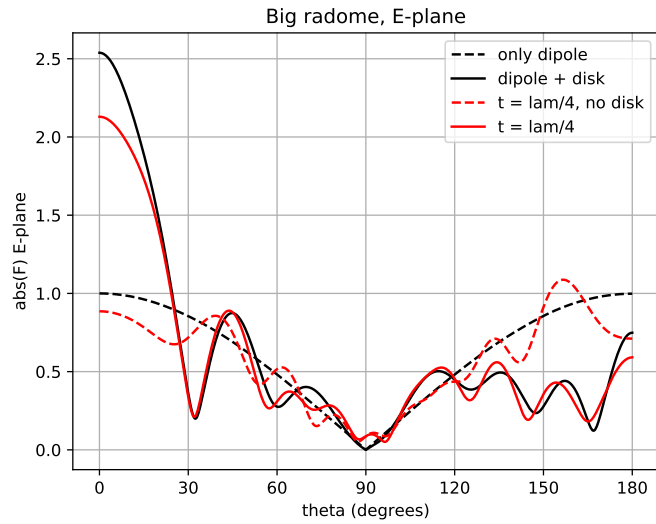
The computation only takes about a minute on a regular laptop. The results are normalized so that the far field amplitude at  $\theta = 0$  for the dipole alone is 1. In Figure 4 the near field distribution is shown. In Figure 5 the far field distribution in the E-plane and H-plane are shown, for the following cases:

- Dipole antenna only.
- Dipole antenna and circular disk PEC reflector.
- Dipole antenna with radome present, no reflector.
- Dipole antenna with reflector and radome present.

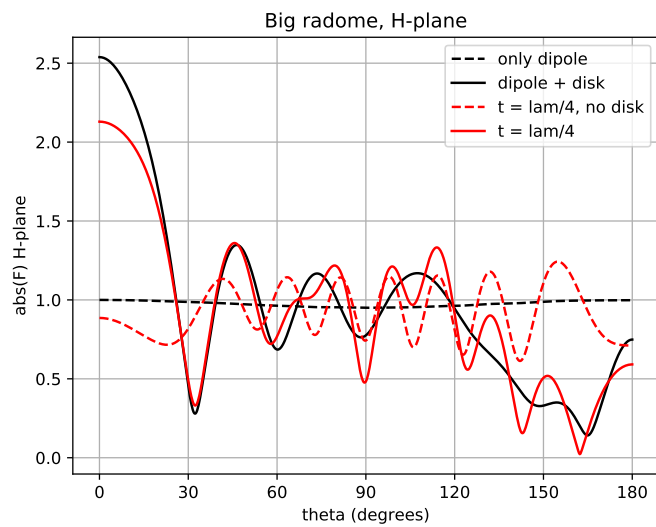
In Figure 5, the dashed black curve shows the radiation pattern of a small dipole: the maximum radiation is in broadside to the dipole, and zero radiation is in the direction of the dipole. The remaining curves show significant influence from the reflector and the radome, illustrating the non-trivial nature of the test case. Several further test cases and comparisons with other methods are given in [2].

## 6 Example: ogive radome

The spherical radome can be analyzed with the method presented in [6], based on expansion in spherical vector waves. However, this method can not easily be extended to non-spherical geometries, whereas the rotationally symmetric approach used here does not have a problem. For instance, we can analyze an ogive-shaped radome, which is a common design for a nose cone radome, see Figure 6. This design



(a)



(b)

Figure 5: Far field of a reflector-backed dipole antenna inside a spherical radome. (a) E-plane, (b) H-plane.

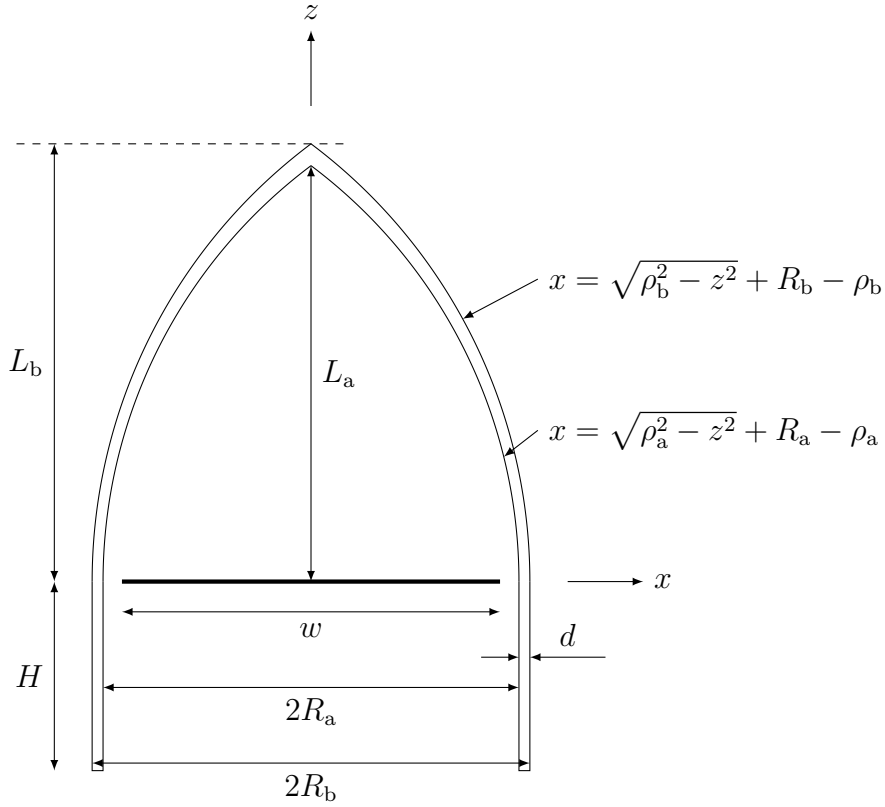


Figure 6: Geometry parameters of the ogive radome, adapted from [https://en.wikipedia.org/wiki/Nose\\_cone\\_design](https://en.wikipedia.org/wiki/Nose_cone_design). The radius of curvature for the ogive parts is computed from the other parameters as  $\rho_{a,b} = (R_{a,b}^2 + L_{a,b}^2)/(2R_{a,b})$ , and the thickness of the radome at the base is  $d = R_b - R_a$ . The antenna width is  $w$ , and the distance between the antenna and the radome is  $d_0 = R_a - w/2$ .

has several features of a realistic radome, such as a pointed tip and non-uniform wall thickness.

The baseline parameters of the radome, corresponding to Figure 6, are chosen as

- $f_0 = 10$  GHz (frequency)
- $\lambda_0 = c_0/f_0$  (wavelength)
- $w = 10\lambda_0 = 0.300$  m (diameter of antenna)
- $d_0 = \lambda_0/2 = 0.0150$  m (distance from antenna to radome)
- $\epsilon_r = 3(1 - 0.01j)$  (relative permittivity of radome)
- $d = \lambda_0/(2 \operatorname{Re} \sqrt{\epsilon_r}) = 8.7$  mm (thickness of radome)
- $\alpha = 2$  (ogive shape factor)
- $R_a = w/2 + d_0 = 0.165$  m



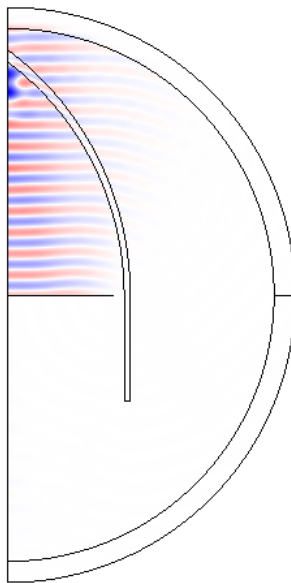


Figure 7: Fields of a cosine-tapered circular antenna inside an ogive-shaped radome,  $w = 10\lambda_0$ .

- $L_a = \alpha R_a = 0.330$  m
- $\rho_a = (R_a^2 + L_a^2)/(2R_a) = 0.412$  m
- $R_b = w/2 + d_0 + d = 0.174$  m
- $L_b = \alpha R_b = 0.347$  m
- $\rho_b = (R_b^2 + L_b^2)/(2R_b) = 0.434$  m
- $H = 5\lambda_0 = 0.150$  m

The antenna is implemented as a linearly polarized circular antenna with a cosine-tapering in the radial direction as described in Section 4, in particular equation (4.1). The baseline antenna is ten wavelengths in diameter, making the radiation highly directive.

Once again, the simulation only takes in the order of a minute on a regular laptop. The limiting factor with respect to radome size is the memory (16 GB were available on the used platform). The near field distribution is shown in Figure 7, where it is seen that the large size of the antenna makes the wave propagate almost purely in the forward direction. It is seen that there is a significant interaction with the pointed tip, where the field distribution is distorted as compared to a propagating plane wave.

In Figure 8, the far fields in the E-plane and the H-plane are given for three different radome sizes, where  $w/\lambda_0 = 10, 30, 50$ . Note that dB-scale is used for the vertical axis in Figure 8, due to the large dynamics involved, and that the two

larger sizes  $w/\lambda_0 = 30, 50$  are run on a platform with larger memory than 16 GB (but using comparable implementations in Comsol). In each subfigure, all results are scaled to the maximum radiation of the antenna without a radome. It is noted the side lobe level is below 20 dB in all cases, and that the insertion loss at  $\theta = 0$  is around 1 dB for  $w = 30\lambda_0$  and  $w = 50\lambda_0$ .

## 7 Conclusions

We have presented a method to compute reference cases for rotationally symmetric radomes using commercial software. Comsol Multiphysics was used as an example since this was readily available at our university, but any software being able to handle rotationally symmetric structures should be possible to use in the same way. The drawback is that in order to reduce the number of azimuthal modes, the excitation needs to be highly symmetrical, typically radiating in the direction of the axis of symmetry. More realistic sources can be treated at the expense of longer simulation time, but does not require more memory since the simulations can be made in sequence and only a small amount of data (the far field amplitude) needs to be saved from each simulation. However, this kind of simulation requires more work to be implemented, and is suggested as a natural follow-up to provide more realistic reference cases for radome simulations.

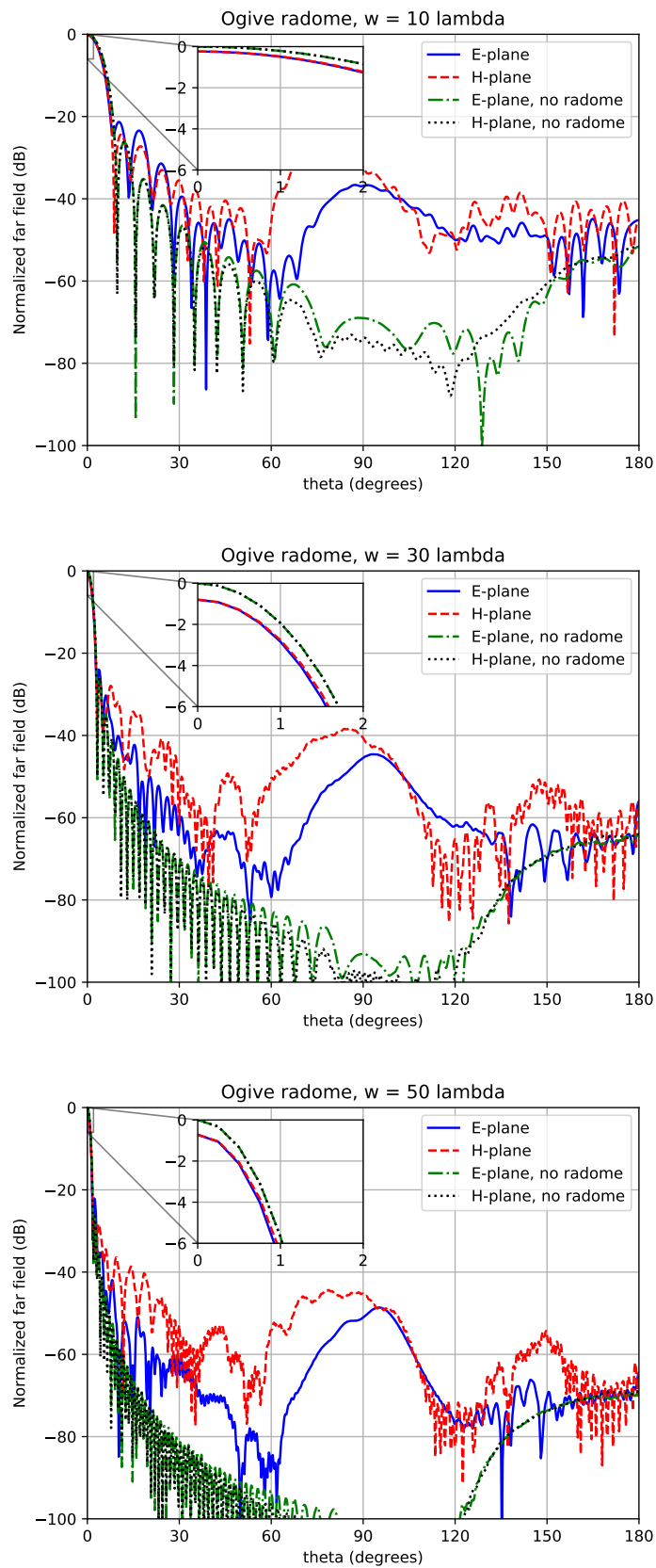


Figure 8: Far field of a cosine-tapered circular antenna inside an ogive-shaped radome for three different sizes:  $w = 10\lambda_0$  (top),  $w = 30\lambda_0$  (center), and  $w = 50\lambda_0$  (bottom).

## A Computation of far field amplitudes

In this Appendix, we give explicit derivations of how the far field amplitudes used in the computational examples can be derived. The general setup of solving Maxwell's equations in a rotationally symmetric geometry is provided in Section 2. There, it is seen that the fields can be represented in cylindrical coordinates  $(\rho, \varphi, z)$  as

$$\mathbf{E}(\mathbf{r}) = \sum_{m=-\infty}^{\infty} [E_{\rho}^{(m)}(\rho, z)\hat{\boldsymbol{\rho}} + E_{\varphi}^{(m)}(\rho, z)\hat{\boldsymbol{\varphi}} + E_z^{(m)}(\rho, z)\hat{\boldsymbol{z}}] e^{-jm\varphi} \quad (\text{A.1})$$

$$\mathbf{H}(\mathbf{r}) = \sum_{m=-\infty}^{\infty} [H_{\rho}^{(m)}(\rho, z)\hat{\boldsymbol{\rho}} + H_{\varphi}^{(m)}(\rho, z)\hat{\boldsymbol{\varphi}} + H_z^{(m)}(\rho, z)\hat{\boldsymbol{z}}] e^{-jm\varphi} \quad (\text{A.2})$$

In this Appendix, we demonstrate how to solve the azimuthal part of the far field integral

$$\mathbf{F}(\hat{\mathbf{k}}) = \frac{jk}{4\pi} \hat{\mathbf{k}} \times \int_S [\mathbf{E}(\mathbf{r}) \times \hat{\mathbf{n}} + \eta_0 \hat{\mathbf{k}} \times (\hat{\mathbf{n}} \times \mathbf{H}(\mathbf{r}))] e^{j\hat{\mathbf{k}} \cdot \mathbf{r}} dS \quad (\text{A.3})$$

for arbitrary azimuthal mode index  $m$ . The radiation direction  $\hat{\mathbf{k}}$  is parametrized by the standard polar angle  $\theta$  and azimuth angle  $\phi$ . Having derived the general case, we also derive expressions for the  $\phi = 0$  and  $\phi = \pi/2$  planes, the axial mode ( $m = 0$ ), and the E-plane and H-plane results for linear polarization synthesized from the  $m = \pm 1$  modes. The computations are provided in detail to show what underlies the resulting formulas.

### A.1 Arbitrary $m$

The fields  $\mathbf{E}^{(m)}(\rho, z)$  and  $\mathbf{H}^{(m)}(\rho, z)$  depend only on  $\rho$  and  $z$ , whereas the  $\varphi$ -dependence is in a factor  $e^{-jm\varphi}$ . Hence, the far field integrals to be computed are proportional to

$$\int_{\rho \in \gamma} \int_{\varphi=0}^{2\pi} [\mathbf{E}^{(m)} \times \hat{\mathbf{n}}] e^{j(\mathbf{k} \cdot \mathbf{r} - m\varphi)} \rho d\varphi dl \quad \text{and} \quad \int_{\rho \in \gamma} \int_{\varphi=0}^{2\pi} [\hat{\mathbf{n}} \times \mathbf{H}^{(m)}] e^{j(\mathbf{k} \cdot \mathbf{r} - m\varphi)} \rho d\varphi dl \quad (\text{A.4})$$

where  $\gamma$  is the curve in the  $\rho$ - $z$  plane where the integral is to be computed,  $\rho$  and  $z$  are coordinates on this curve, with  $dl$  as a line element. The unit normal vector is  $\hat{\mathbf{n}} = n_{\rho}\hat{\boldsymbol{\rho}} + n_z\hat{\boldsymbol{z}}$ , meaning the electric and magnetic tangential fields are (using  $\hat{\boldsymbol{\rho}} \times \hat{\boldsymbol{\varphi}} = \hat{\boldsymbol{z}}$ )

$$\mathbf{E}^{(m)} \times \hat{\mathbf{n}} = (n_{\rho}E_z^{(m)} - n_zE_{\rho}^{(m)})\hat{\boldsymbol{\varphi}} - n_{\rho}E_{\varphi}^{(m)}\hat{\boldsymbol{z}} + n_zE_{\varphi}^{(m)}\hat{\boldsymbol{\rho}} \quad (\text{A.5})$$

$$\hat{\mathbf{n}} \times \mathbf{H}^{(m)} = (-n_{\rho}H_z^{(m)} + n_zH_{\rho}^{(m)})\hat{\boldsymbol{\varphi}} + n_{\rho}H_{\varphi}^{(m)}\hat{\boldsymbol{z}} - n_zH_{\varphi}^{(m)}\hat{\boldsymbol{\rho}} \quad (\text{A.6})$$

The unit vectors are

$$\hat{\boldsymbol{\rho}} = \hat{\mathbf{x}} \cos \varphi + \hat{\mathbf{y}} \sin \varphi \quad (\text{A.7})$$

$$\hat{\boldsymbol{\varphi}} = -\hat{\mathbf{x}} \sin \varphi + \hat{\mathbf{y}} \cos \varphi \quad (\text{A.8})$$

meaning the tangential fields are

$$\mathbf{E}^{(m)} \times \hat{\mathbf{n}} = [n_z E_\varphi^{(m)} \cos(\varphi) - (n_\rho E_z^{(m)} - n_z E_\rho^{(m)}) \sin(\varphi)] \hat{\mathbf{x}} \quad (\text{A.9})$$

$$+ [n_z E_\varphi^{(m)} \sin(\varphi) + (n_\rho E_z^{(m)} - n_z E_\rho^{(m)}) \cos(\varphi)] \hat{\mathbf{y}} - n_\rho E_\varphi^{(m)} \hat{\mathbf{z}} \quad (\text{A.10})$$

$$\hat{\mathbf{n}} \times \mathbf{H}^{(m)} = -[n_z H_\varphi^{(m)} \cos(\varphi) - (n_\rho H_z^{(m)} - n_z H_\rho^{(m)}) \sin(\varphi)] \hat{\mathbf{x}} \quad (\text{A.11})$$

$$- [n_z H_\varphi^{(m)} \sin(\varphi) + (n_\rho H_z^{(m)} - n_z H_\rho^{(m)}) \cos(\varphi)] \hat{\mathbf{y}} + n_\rho H_\varphi^{(m)} \hat{\mathbf{z}} \quad (\text{A.12})$$

The phase factor is

$$e^{j(\mathbf{k} \cdot \mathbf{r} - m\varphi)} = e^{j(\mathbf{k} \cdot (\rho \hat{\boldsymbol{\rho}} + z \hat{\mathbf{z}}) - m\varphi)} = e^{j(k\rho \sin \theta \cos(\varphi - \phi) - m\varphi)} e^{jkz \cos \theta} \quad (\text{A.13})$$

where we used  $\mathbf{k} \cdot \mathbf{r} = k\rho \sin \theta \cos(\varphi - \phi) + kz \cos \theta$ , with  $\mathbf{k} = k[\sin \theta(\cos \phi \hat{\mathbf{x}} + \sin \phi \hat{\mathbf{y}}) + \cos \theta \hat{\mathbf{z}}]$ . Thus, the typical azimuth integrals to be computed are:

$$\begin{aligned}
\int_0^{2\pi} e^{j(k\rho \sin \theta \cos(\varphi - \phi) - m\varphi)} d\varphi &\stackrel{\varphi' = \varphi - \phi + \pi/2}{=} \int_0^{2\pi} e^{j(k\rho \sin \theta \cos(\varphi' - \pi/2) - m(\varphi' + \phi - \pi/2))} d\varphi' \\
&= e^{-jm(\phi - \pi/2)} \int_{-\pi}^{\pi} e^{j(k\rho \sin \theta \sin(\varphi') - m\varphi')} d\varphi' \\
&= e^{-jm\phi} j^m 2\pi J_m(k\rho \sin \theta) \\
&= 2\pi j^m e^{-jm\phi} A_m
\end{aligned} \tag{A.14}$$

$$\begin{aligned}
\int_0^{2\pi} \sin(\varphi) e^{j(k\rho \cos(\varphi - \phi) - m\varphi)} d\varphi &= \frac{1}{2j} \left[ \int_0^{2\pi} e^{j(k\rho \sin \theta \cos(\varphi - \phi) - (m-1)\varphi)} d\varphi \right. \\
&\quad \left. - \int_0^{2\pi} e^{j(k\rho \sin \theta \cos(\varphi - \phi) - (m+1)\varphi)} d\varphi \right] \\
&= \frac{1}{2j} \left[ e^{-j(m-1)\phi} j^{m-1} 2\pi J_{m-1}(k\rho \sin \theta) \right. \\
&\quad \left. - e^{-j(m+1)\phi} j^{m+1} 2\pi J_{m+1}(k\rho \sin \theta) \right] \\
&= 2\pi j^m e^{-jm\phi} \frac{1}{2j} [e^{j\phi} j^{-1} J_{m-1}(k\rho \sin \theta) - e^{-j\phi} j J_{m+1}(k\rho \sin \theta)] \\
&= -2\pi j^m e^{-jm\phi} \frac{1}{2} [e^{j\phi} J_{m-1}(k\rho \sin \theta) + e^{-j\phi} J_{m+1}(k\rho \sin \theta)] \\
&= -2\pi j^m e^{-jm\phi} S_m
\end{aligned} \tag{A.15}$$

$$\begin{aligned}
\int_0^{2\pi} \cos(\varphi) e^{j(k\rho \cos(\varphi - \phi) - m\varphi)} d\varphi &= \frac{1}{2} \left[ \int_0^{2\pi} e^{j(k\rho \sin \theta \cos(\varphi - \phi) - (m-1)\varphi)} d\varphi \right. \\
&\quad \left. + \int_0^{2\pi} e^{j(k\rho \sin \theta \cos(\varphi - \phi) - (m+1)\varphi)} d\varphi \right] \\
&= \frac{1}{2} \left[ e^{-j(m-1)\phi} j^{m-1} 2\pi J_{m-1}(k\rho \sin \theta) \right. \\
&\quad \left. + e^{-j(m+1)\phi} j^{m+1} 2\pi J_{m+1}(k\rho \sin \theta) \right] \\
&= 2\pi j^m e^{-jm\phi} \frac{1}{2} [e^{j\phi} j^{-1} J_{m-1}(k\rho \sin \theta) + e^{-j\phi} j J_{m+1}(k\rho \sin \theta)] \\
&= -2\pi j^m e^{-jm\phi} \frac{j}{2} [e^{j\phi} J_{m-1}(k\rho \sin \theta) - e^{-j\phi} J_{m+1}(k\rho \sin \theta)] \\
&= -2\pi j^m e^{-jm\phi} C_m
\end{aligned} \tag{A.16}$$

where we used the representation [1, p. 9.1.21]

$$J_m(z) = \frac{1}{\pi} \int_0^\pi \cos(z \sin \theta - m\theta) d\theta = \frac{1}{2\pi} \int_{-\pi}^\pi e^{j(z \sin \theta - m\theta)} d\theta = \frac{1}{2\pi} \int_0^{2\pi} e^{j(z \sin \theta - m\theta)} d\theta \tag{A.17}$$

where  $m$  is a positive integer or zero. Thus, after integration over  $\varphi$ , we have (premultiplying with the factor  $1/(2\pi j^m e^{j(kz \cos \theta - m\phi)})$  for simplicity)

$$\begin{aligned} & \frac{1}{2\pi j^m e^{j(kz \cos \theta - m\phi)}} \int_0^{2\pi} [\mathbf{E}^{(m)} \times \hat{\mathbf{n}}] e^{j(\mathbf{k} \cdot \mathbf{r} - m\varphi)} d\varphi \\ &= - [n_z E_\varphi^{(m)} C_m - (n_\rho E_z^{(m)} - n_z E_\rho^{(m)}) S_m] \hat{\mathbf{x}} \\ & - [n_z E_\varphi^{(m)} S_m + (n_\rho E_z^{(m)} - n_z E_\rho^{(m)}) C_m] \hat{\mathbf{y}} - n_\rho E_\varphi^{(m)} A_m \hat{\mathbf{z}} \quad (\text{A.18}) \end{aligned}$$

and

$$\begin{aligned} & \frac{1}{2\pi j^m e^{j(kz z - m\phi)}} \int_0^{2\pi} [\hat{\mathbf{n}} \times \mathbf{H}^{(m)}] e^{j(\mathbf{k} \cdot \mathbf{r} - m\varphi)} d\varphi \\ &= [n_z H_\varphi^{(m)} C_m - (n_\rho H_z^{(m)} - n_z H_\rho^{(m)}) S_m] \hat{\mathbf{x}} \\ & + [n_z H_\varphi^{(m)} S_m + (n_\rho H_z^{(m)} - n_z H_\rho^{(m)}) C_m] \hat{\mathbf{y}} + n_\rho H_\varphi^{(m)} A_m \hat{\mathbf{z}} \quad (\text{A.19}) \end{aligned}$$

The remaining cross products are (rewriting  $\hat{\mathbf{x}}$ ,  $\hat{\mathbf{y}}$ , and  $\hat{\mathbf{z}}$  in terms of  $(\theta, \phi)$  as the polar angle and azimuth angle in the direction  $\hat{\mathbf{k}}$ )

$$\hat{\mathbf{k}} \times \hat{\mathbf{x}} = \hat{\mathbf{k}} \times (\hat{\mathbf{k}} \sin \theta \cos \phi + \hat{\boldsymbol{\theta}} \cos \theta \cos \phi - \hat{\boldsymbol{\phi}} \sin \phi) = \hat{\boldsymbol{\phi}} \cos \theta \cos \phi + \hat{\boldsymbol{\theta}} \sin \phi \quad (\text{A.20})$$

$$\hat{\mathbf{k}} \times \hat{\mathbf{y}} = \hat{\mathbf{k}} \times (\hat{\mathbf{k}} \sin \theta \sin \phi + \hat{\boldsymbol{\theta}} \cos \theta \sin \phi + \hat{\boldsymbol{\phi}} \cos \phi) = \hat{\boldsymbol{\phi}} \cos \theta \sin \phi - \hat{\boldsymbol{\theta}} \cos \phi \quad (\text{A.21})$$

$$\hat{\mathbf{k}} \times \hat{\mathbf{z}} = \hat{\mathbf{k}} \times (\hat{\mathbf{k}} \cos \theta - \hat{\boldsymbol{\theta}} \sin \theta) = -\hat{\boldsymbol{\phi}} \sin \theta \quad (\text{A.22})$$

$$\begin{aligned} \hat{\mathbf{k}} \times (\hat{\mathbf{k}} \times \hat{\mathbf{x}}) &= [\hat{\mathbf{k}}\hat{\mathbf{k}} - \mathbf{1}] \cdot (\hat{\mathbf{k}} \sin \theta \cos \phi + \hat{\boldsymbol{\theta}} \cos \theta \cos \phi - \hat{\boldsymbol{\phi}} \sin \phi) \\ &= -\hat{\boldsymbol{\theta}} \cos \theta \cos \phi + \hat{\boldsymbol{\phi}} \sin \phi \quad (\text{A.23}) \end{aligned}$$

$$\begin{aligned} \hat{\mathbf{k}} \times (\hat{\mathbf{k}} \times \hat{\mathbf{y}}) &= [\hat{\mathbf{k}}\hat{\mathbf{k}} - \mathbf{1}] \cdot (\hat{\mathbf{k}} \sin \theta \sin \phi + \hat{\boldsymbol{\theta}} \cos \theta \sin \phi + \hat{\boldsymbol{\phi}} \cos \phi) \\ &= -\hat{\boldsymbol{\theta}} \cos \theta \sin \phi - \hat{\boldsymbol{\phi}} \cos \phi \quad (\text{A.24}) \end{aligned}$$

$$\hat{\mathbf{k}} \times (\hat{\mathbf{k}} \times \hat{\mathbf{z}}) = [\hat{\mathbf{k}}\hat{\mathbf{k}} - \mathbf{1}] \cdot (\hat{\mathbf{k}} \cos \theta - \hat{\boldsymbol{\theta}} \sin \theta) = \hat{\boldsymbol{\theta}} \sin \theta \quad (\text{A.25})$$

Bringing it all together, the far field is then

$$\begin{aligned}
\mathbf{F}^{(m)}(\theta, \phi) &= \frac{j^m k}{4\pi} \hat{\mathbf{k}} \times \int_S \left[ \mathbf{E}^{(m)}(\mathbf{r}) \times \hat{\mathbf{n}} + \eta_0 \hat{\mathbf{k}} \times (\hat{\mathbf{n}} \times \mathbf{H}^{(m)}(\mathbf{r})) \right] e^{j(k\hat{\mathbf{k}} \cdot \mathbf{r} - m\varphi)} dS \\
&= \frac{j^m k}{2} e^{-jm\phi} \int_{\rho \in \gamma} \left( - [n_z E_\varphi^{(m)} C_m - (n_\rho E_z^{(m)} - n_z E_\rho^{(m)}) S_m] \underbrace{(\hat{\phi} \cos \theta \cos \phi + \hat{\theta} \sin \phi)}_{=\hat{\mathbf{k}} \times \hat{\mathbf{x}}} \right. \\
&\quad - [n_z E_\varphi^{(m)} S_m + (n_\rho E_z^{(m)} - n_z E_\rho^{(m)}) C_m] \underbrace{(\hat{\phi} \cos \theta \sin \phi - \hat{\theta} \cos \phi)}_{=\hat{\mathbf{k}} \times \hat{\mathbf{y}}} \\
&\quad \left. - n_\rho E_\varphi^{(m)} A_m \underbrace{(-\hat{\phi} \sin \theta)}_{=\hat{\mathbf{k}} \times \hat{\mathbf{z}}} \right) \\
&\quad + \eta_0 [n_z H_\varphi^{(m)} C_m - (n_\rho H_z^{(m)} - n_z H_\rho^{(m)}) S_m] \underbrace{(-\hat{\theta} \cos \theta \cos \phi + \hat{\phi} \sin \phi)}_{=\hat{\mathbf{k}} \times (\hat{\mathbf{k}} \times \hat{\mathbf{x}})} \\
&\quad + \eta_0 [n_z H_\varphi^{(m)} S_m + (n_\rho H_z^{(m)} - n_z H_\rho^{(m)}) C_m] \underbrace{(-\hat{\theta} \cos \theta \sin \phi - \hat{\phi} \cos \phi)}_{=\hat{\mathbf{k}} \times (\hat{\mathbf{k}} \times \hat{\mathbf{y}})} \\
&\quad \left. + \eta_0 n_\rho H_\varphi^{(m)} A_m \underbrace{\hat{\theta} \sin \theta}_{=\hat{\mathbf{k}} \times (\hat{\mathbf{k}} \times \hat{\mathbf{z}})} \right) e^{jkz \cos \theta} \rho d\ell \quad (\text{A.26})
\end{aligned}$$

Our final result is then

$$\begin{aligned}
\mathbf{F}^{(m)}(\theta, \phi) &= \hat{\theta} \frac{j^m k}{2} e^{-jm\phi} \int_{\rho \in \gamma} \left\{ - [C_m n_z E_\varphi^{(m)} - S_m (n_\rho E_z^{(m)} - n_z E_\rho^{(m)})] \sin \phi \right. \\
&\quad + [S_m n_z E_\varphi^{(m)} + C_m (n_\rho E_z^{(m)} - n_z E_\rho^{(m)})] \cos \phi \\
&\quad - \eta_0 [C_m n_z H_\varphi^{(m)} - S_m (n_\rho H_z^{(m)} - n_z H_\rho^{(m)})] \cos \theta \cos \phi \\
&\quad - \eta_0 [S_m n_z H_\varphi^{(m)} + C_m (n_\rho H_z^{(m)} - n_z H_\rho^{(m)})] \cos \theta \sin \phi \\
&\quad \left. + \eta_0 A_m n_\rho H_\varphi^{(m)} \sin \theta \right\} e^{jkz \cos \theta} \rho d\ell \\
&\quad + \hat{\phi} \frac{j^m k}{2} e^{-jm\phi} \int_{\rho \in \gamma} \left\{ - [C_m n_z E_\varphi^{(m)} - S_m (n_\rho E_z^{(m)} - n_z E_\rho^{(m)})] \cos \theta \cos \phi \right. \\
&\quad - [S_m n_z E_\varphi^{(m)} + C_m (n_\rho E_z^{(m)} - n_z E_\rho^{(m)})] \cos \theta \sin \phi \\
&\quad + A_m n_\rho E_\varphi^{(m)} \sin \theta \\
&\quad + \eta_0 [C_m n_z H_\varphi^{(m)} - S_m (n_\rho H_z^{(m)} - n_z H_\rho^{(m)})] \sin \phi \\
&\quad \left. - \eta_0 [S_m n_z H_\varphi^{(m)} + C_m (n_\rho H_z^{(m)} - n_z H_\rho^{(m)})] \cos \phi \right\} e^{jkz \cos \theta} \rho d\ell \quad (\text{A.27})
\end{aligned}$$

which gives the far field amplitude for azimuthal mode  $m$  at any direction  $(\theta, \phi)$ .

## A.2 Expressions for angular cuts

It is often desired to consider (A.27) in the two typical planes  $\phi = 0$  and  $\phi = \pi/2$ , often (but not necessarily) corresponding the E-plane and H-plane of the radiation.



Using the recurrence relations [1, p. 9.1.27]

$$J_{m-1}(z) + J_{m+1}(z) = \frac{2m}{z} J_m(z) \quad (\text{A.28})$$

$$J_{m-1}(z) - J_{m+1}(z) = 2 J'_m(z) \quad (\text{A.29})$$

the original expressions for  $A_m$ ,  $S_m$ , and  $C_m$  can then be written as

$$A_m = J_m(k\rho \sin \theta) \quad (\text{A.30})$$

$$S_m = \frac{1}{2} [e^{j\phi} J_{m-1}(k\rho \sin \theta) + e^{-j\phi} J_{m+1}(k\rho \sin \theta)] = \begin{cases} \frac{m J_m(k\rho \sin \theta)}{k\rho \sin \theta} & \phi = 0 \\ j J'_m(k\rho \sin \theta) & \phi = \pi/2 \end{cases} \quad (\text{A.31})$$

$$C_m = \frac{j}{2} [e^{j\phi} J_{m-1}(k\rho \sin \theta) - e^{-j\phi} J_{m+1}(k\rho \sin \theta)] = \begin{cases} j J'_m(k\rho \sin \theta) & \phi = 0 \\ -\frac{m J_m(k\rho \sin \theta)}{k\rho \sin \theta} & \phi = \pi/2 \end{cases} \quad (\text{A.32})$$

We also note that

$$j^m e^{-jm\phi} = \begin{cases} j^m & \phi = 0 \\ 1 & \phi = \pi/2 \end{cases} \quad (\text{A.33})$$

In the plane  $\phi = 0$ ,  $0 < \theta < \pi$ , the far field pattern (A.27) then becomes (this plane corresponds to the form provided in [3], with the difference that  $m \rightarrow -m$  and  $\mathbf{F} \rightarrow -\mathbf{F}$  in their work)

$$\begin{aligned} & \mathbf{F}^{(m)}(\theta, \phi = 0) \\ &= \hat{\boldsymbol{\theta}} \frac{jk}{2} j^m \int_{\rho \in \gamma} \left\{ \left[ \frac{m J_m(k\rho \sin \theta)}{k\rho \sin \theta} n_z E_\varphi^{(m)} + j J'_m(k\rho \sin \theta) (n_\rho E_z^{(m)} - n_z E_\rho^{(m)}) \right] \right. \\ & \quad - \eta_0 \left[ j J'_m(k\rho \sin \theta) n_z H_\varphi^{(m)} - \frac{m J_m(k\rho \sin \theta)}{k\rho \sin \theta} (n_\rho H_z^{(m)} - n_z H_\rho^{(m)}) \right] \cos \theta \\ & \quad \left. + \eta_0 J_m(k\rho \sin \theta) n_\rho H_\varphi^{(m)} \sin \theta \right\} e^{jkz \cos \theta} \rho \, d\ell \\ &+ \hat{\boldsymbol{\phi}} \frac{jk}{2} j^m \int_{\rho \in \gamma} \left\{ \left[ -j J'_m(k\rho \sin \theta) n_z E_\varphi^{(m)} + \frac{m J_m(k\rho \sin \theta)}{k\rho \sin \theta} (n_\rho E_z^{(m)} - n_z E_\rho^{(m)}) \right] \cos \theta \right. \\ & \quad \left. + J_m(k\rho \sin \theta) n_\rho E_\varphi^{(m)} \sin \theta \right. \\ & \quad \left. - \eta_0 \left[ \frac{m J_m(k\rho \sin \theta)}{k\rho \sin \theta} n_z H_\varphi^{(m)} + j J'_m(k\rho \sin \theta) (n_\rho H_z^{(m)} - n_z H_\rho^{(m)}) \right] \right\} e^{jkz \cos \theta} \rho \, d\ell \end{aligned} \quad (\text{A.34})$$

In the plane  $\phi = \pi/2$ ,  $0 < \theta < \pi$ , we have

$$\begin{aligned}
& \mathbf{F}^{(m)}(\theta, \phi = \pi/2) \\
&= \hat{\theta} \frac{jk}{2} \int_{\rho \in \gamma} \left\{ \left[ \frac{m J_m(k\rho \sin \theta)}{k\rho \sin \theta} n_z E_\varphi^{(m)} + j J'_m(k\rho \sin \theta) (n_\rho E_z^{(m)} - n_z E_\rho^{(m)}) \right] \right. \\
&\quad - \eta_0 \left[ j J'_m(k\rho \sin \theta) n_z H_\varphi^{(m)} - \frac{m J_m(k\rho \sin \theta)}{k\rho \sin \theta} (n_\rho H_z^{(m)} - n_z H_\rho^{(m)}) \right] \cos \theta \\
&\quad \left. + \eta_0 J_m(k\rho \sin \theta) n_\rho H_\varphi^{(m)} \sin \theta \right\} e^{jkz \cos \theta} \rho d\ell \\
&+ \hat{\phi} \frac{jk}{2} \int_{\rho \in \gamma} \left\{ - \left[ j J'_m(k\rho \sin \theta) n_z E_\varphi^{(m)} - \frac{m J_m(k\rho \sin \theta)}{k\rho \sin \theta} (n_\rho E_z^{(m)} - n_z E_\rho^{(m)}) \right] \cos \theta \right. \\
&\quad \left. + J_m(k\rho \sin \theta) n_\rho E_\varphi^{(m)} \sin \theta \right. \\
&\quad \left. + \eta_0 \left[ - \frac{m J_m(k\rho \sin \theta)}{k\rho \sin \theta} n_z H_\varphi^{(m)} - j J'_m(k\rho \sin \theta) (n_\rho H_z^{(m)} - n_z H_\rho^{(m)}) \right] \right\} e^{jkz \cos \theta} \rho d\ell
\end{aligned} \tag{A.35}$$

These expressions apply to any mode  $m$ .

### A.3 Axial fields, $m = 0$

A common excitation is an axisymmetric current, which generates the  $m = 0$  mode. For  $m = 0$ , we have (using  $J_{-1}(z) = -J_1(z)$ )

$$A_0 = J_0(k\rho \sin \theta) \tag{A.36}$$

$$S_0 = \frac{1}{2} [e^{j\phi} J_{-1}(k\rho \sin \theta) + e^{-j\phi} J_1(k\rho \sin \theta)] = -j \sin \phi J_1(k\rho \sin \theta) \tag{A.37}$$

$$C_0 = \frac{j}{2} [e^{j\phi} J_{-1}(k\rho \sin \theta) - e^{-j\phi} J_1(k\rho \sin \theta)] = -j \cos \phi J_1(k\rho \sin \theta) \tag{A.38}$$

The farfield pattern (A.27) is then

$$\begin{aligned}
\mathbf{F}^{(0)}(\theta, \phi) &= \hat{\boldsymbol{\theta}} \frac{jk}{2} \int_{\rho \in \gamma} \left\{ -[-j \cos \phi n_z E_\varphi^{(0)} + j \sin \phi (n_\rho E_z^{(0)} - n_z E_\rho^{(0)})] J_1(k\rho \sin \theta) \sin \phi \right. \\
&\quad + [-j \sin \phi n_z E_\varphi^{(0)} - j \cos \phi (n_\rho E_z^{(0)} - n_z E_\rho^{(0)})] J_1(k\rho \sin \theta) \cos \phi \\
&\quad - \eta_0 [-j \cos \phi n_z H_\varphi^{(0)} + j \sin \phi (n_\rho H_z^{(0)} - n_z H_\rho^{(0)})] J_1(k\rho \sin \theta) \cos \theta \cos \phi \\
&\quad - \eta_0 [-j \sin \phi n_z H_\varphi^{(0)} - j \cos \phi (n_\rho H_z^{(0)} - n_z H_\rho^{(0)})] J_1(k\rho \sin \theta) \cos \theta \sin \phi \\
&\quad \left. + \eta_0 J_0(k\rho \sin \theta) n_\rho H_\varphi^{(0)} \sin \theta \right\} e^{jkz \cos \theta} \rho d\ell \\
&+ \hat{\boldsymbol{\phi}} \frac{jk}{2} \int_{\rho \in \gamma} \left\{ -[-j \cos \phi n_z E_\varphi^{(0)} + j \sin \phi (n_\rho E_z^{(0)} - n_z E_\rho^{(0)})] J_1(k\rho \sin \theta) \cos \theta \cos \phi \right. \\
&\quad - [-j \sin \phi n_z E_\varphi^{(0)} - j \cos \phi (n_\rho E_z^{(0)} - n_z E_\rho^{(0)})] J_1(k\rho \sin \theta) \cos \theta \sin \phi \\
&\quad \quad + J_0(k\rho \sin \theta) n_\rho E_\varphi^{(0)} \sin \theta \\
&\quad + \eta_0 [-j \cos \phi n_z H_\varphi^{(0)} + j \sin \phi (n_\rho H_z^{(0)} - n_z H_\rho^{(0)})] J_1(k\rho \sin \theta) \sin \phi \\
&\quad \left. - \eta_0 [-j \sin \phi n_z H_\varphi^{(0)} - j \cos \phi (n_\rho H_z^{(0)} - n_z H_\rho^{(0)})] J_1(k\rho \sin \theta) \cos \phi \right\} e^{jkz \cos \theta} \rho d\ell \\
&= \hat{\boldsymbol{\theta}} \frac{jk}{2} \int_{\rho \in \gamma} \left\{ -j (n_\rho E_z^{(0)} - n_z E_\rho^{(0)}) J_1(k\rho \sin \theta) \right. \\
&\quad \quad + j \eta_0 n_z H_\varphi^{(0)} J_1(k\rho \sin \theta) \cos \theta \\
&\quad \left. + \eta_0 J_0(k\rho \sin \theta) n_\rho H_\varphi^{(0)} \sin \theta \right\} e^{jkz \cos \theta} \rho d\ell \\
&\quad + \hat{\boldsymbol{\phi}} \frac{jk}{2} \int_{\rho \in \gamma} \left\{ j n_z E_\varphi^{(0)} J_1(k\rho \sin \theta) \cos \theta \right. \\
&\quad \quad + J_0(k\rho \sin \theta) n_\rho E_\varphi^{(0)} \sin \theta \\
&\quad \left. + j \eta_0 (n_\rho H_z^{(0)} - n_z H_\rho^{(0)}) J_1(k\rho \sin \theta) \right\} e^{jkz \cos \theta} \rho d\ell \quad (\text{A.39})
\end{aligned}$$

It is seen that there is no dependence on the angle  $\phi$  (except for the direction of the  $\hat{\boldsymbol{\phi}}$  unit vector), reflecting the rotational symmetry of the  $m = 0$  mode.

#### A.4 Synthesized linear polarization, $m = 1$

We finally turn to synthesizing a linear polarization by combining the  $m = +1$  and the  $m = -1$  modes, as outlined in Section 2.2. The synthesized linear polarization has the far field

$$\mathbf{F}_{\text{LP}}^{(1)}(\theta, \phi) = \mathbf{F}^{(1)}(\theta, \phi) + \mathbf{F}^{(-1)}(\theta, \phi) \quad (\text{A.40})$$

using the following parities for  $m = \pm 1$ :

$$(E_\rho^{(+m)}, E_z^{(+m)}, H_\varphi^{(+m)}) = (E_\rho^{(-m)}, E_z^{(-m)}, H_\varphi^{(-m)}) \quad (\text{A.41})$$

$$(E_\varphi^{(+m)}, H_\rho^{(+m)}, H_z^{(+m)}) = -(E_\varphi^{(-m)}, H_\rho^{(-m)}, H_z^{(-m)}) \quad (\text{A.42})$$

$$J'_m(z) = -J'_{-m}(z) \quad (\text{A.43})$$

$$m J_m(z) = (-m) J_{-m}(z) \quad (\text{A.44})$$

The expressions simplify in the planes  $\phi = 0$  (E-plane) and  $\phi = \pi/2$  (H-plane). Taking odd and even parities into account, we have in the E-plane ( $\phi = 0, 0 < \theta < \pi$ )

$$\begin{aligned} \mathbf{F}_E(\theta) &= \mathbf{F}^{(1)}(\theta, \phi = 0) + \mathbf{F}^{(-1)}(\theta, \phi = 0) \\ &= \hat{\boldsymbol{\theta}} \frac{jk}{2} \int_{\rho \in \gamma} \left\{ \left[ \frac{J_1(k\rho \sin \theta)}{k\rho \sin \theta} n_z E_\varphi^{(1)} + j J_1'(k\rho \sin \theta) (n_\rho E_z^{(1)} - n_z E_\rho^{(1)}) \right] \right. \\ &\quad \left. - \eta_0 \left[ j J_1'(k\rho \sin \theta) n_z H_\varphi^{(1)} - \frac{J_1(k\rho \sin \theta)}{k\rho \sin \theta} (n_\rho H_z^{(1)} - n_z H_\rho^{(1)}) \right] \cos \theta \right. \\ &\quad \left. + \eta_0 J_1(k\rho \sin \theta) n_\rho H_\varphi^{(1)} \sin \theta \right\} e^{jkz \cos \theta} \rho d\ell \quad (\text{A.45}) \end{aligned}$$

In the H-plane ( $\phi = \pi/2, 0 < \theta < \pi$ ), we have

$$\begin{aligned} \mathbf{F}_H(\theta) &= \mathbf{F}^{(1)}(\theta, \phi = \pi/2) + \mathbf{F}^{(-1)}(\theta, \phi = \pi/2) \\ &= \hat{\boldsymbol{\phi}} \frac{jk}{2} \int_{\rho \in \gamma} \left\{ - \left[ j J_1'(k\rho \sin \theta) n_z E_\varphi^{(1)} - \frac{J_1(k\rho \sin \theta)}{k\rho \sin \theta} (n_\rho E_z^{(1)} - n_z E_\rho^{(1)}) \right] \cos \theta \right. \\ &\quad \left. + J_1(k\rho \sin \theta) n_\rho E_\varphi^{(1)} \sin \theta \right. \\ &\quad \left. + \eta_0 \left[ - \frac{J_1(k\rho \sin \theta)}{k\rho \sin \theta} n_z H_\varphi^{(1)} - j J_1'(k\rho \sin \theta) (n_\rho H_z^{(1)} - n_z H_\rho^{(1)}) \right] \right\} e^{jkz \cos \theta} \rho d\ell \quad (\text{A.46}) \end{aligned}$$

It is seen that the far field is polarized purely in the  $\hat{\boldsymbol{\theta}}$ -direction in the E-plane, and purely in the  $\hat{\boldsymbol{\phi}}$ -direction in the H-plane. This is due to the linearly polarized excitation and the rotational symmetry.

## References

- [1] M. Abramowitz and I. A. Stegun, eds. “Handbook of Mathematical Functions”. Applied Mathematics Series No. 55. National Bureau of Standards, 1970.
- [2] M. Andersson and S. Poulsen. Tech. rep. 301553776. Saab Dynamics, 2021.
- [3] C. Ciraci, Y. Urzhumov, and D. R. Smith. “Far-field analysis of axially symmetric three-dimensional directional cloaks”. *Optics express* 21 (8) (2013): pp. 9397–9406.
- [4] D. J. Kozakoff. “Analysis of Radome-Enclosed Antennas”. Artech House, 1997.
- [5] G. Kristensson. *Verification of radome problems—Part I*. Tech. rep. LUTEDX/(TEAT-7262)/1-30/(2018). Dept Electrical and Information Technology, Lund University, Sweden, 2018.
- [6] G. Kristensson. *Verification of radome problems—Part II*. Tech. rep. LUTEDX/(TEAT-7270)/1-26/(2020). Dept Electrical and Information Technology, Lund University, Sweden, 2020.
- [7] S. Poulsen. “Stealth radomes”. PhD thesis. Lund University, 2006.